ACS EARTH AND SPACE CHEMISTRY

Open Access

http://pubs.acs.org/journal/aesccq

Article

Redox Cycling of Tetrahedral Iron Drives the Fenton Reactivity of Chrysotile Asbestos

Martin Walter, Walter D. C. Schenkeveld,* Gerald Geroldinger, Lars Gille, and Stephan M. Kraemer

Cite This: *ACS Earth Space Chem.* 2024, 8, 1−13

Read Online

ACCESS | Metrics & More | Article Recommendations | Supporting Information

ABSTRACT: Chrysotile asbestos is a carcinogenic fibrous mineral. Its pathogenicity is partly governed by the ability of Fe on the fiber surface to catalyze the Fenton reduction of H_2O_2 (which is produced during inflammatory processes) to form the highly toxic hydroxyl radical ($HO^{\bullet}$). Recently, tetrahedrally coordinated Fe (Fe_{tet}) in the fibers' Si sheets was identified as the principal Fe species to catalyze this process. However, as only ferric Fe_{tet} ($Fe^{3+}{}_{tet}$) substitutes Si tetrahedra in chrysotile, Fe_{tet} needs to redox cycle to ferrous Fe_{tet} ($Fe^{2+}{}_{tet}$) to facilitate fiber-mediated reductions of H_2O_2 to $HO^{\bullet}$. This redox cycling has never been experimentally investigated. Here we demonstrate, by consecutive ascorbate and O_2 treatments, that structural Fe_{tet} in exposed Si sheets of chrysotile fibers can redox cycle between $Fe^{3+}{}_{tet}$ and $Fe^{2+}{}_{tet}$. Reduction, back-oxidation, and rereduction of $Fe^{3+}{}_{tet}$ did not labilize the exposed Si sheet and, consequently, did not promote fiber dissolution. However, in the presence of H_2O_2, prolonged redox cycling of Fe_{tet} increased fiber dissolution, presumably by accelerating Fe_{tet} dissolution and subsequent labilization of the exposed Si sheet. Chrysotile fibers for which the concentration of Fe_{tet} surface sites undergoing redox cycling was lowered through selective Fe removal showed a rebound in $Fe^{3+}{}_{tet}$ surface site concentration and associated Fenton reactivity once $Fe^{3+}{}_{tet}$-depleted Si sheets were dissolved off from the fiber surfaces. To conclude, our results demonstrate that redox cycling of Fe_{tet} on chrysotile surfaces produces $Fe^{2+}{}_{tet}$ surface sites, which, as the ultimate Fenton reactive iron species on chrysotile, contribute to the fibers' adverse chemical reactivity.

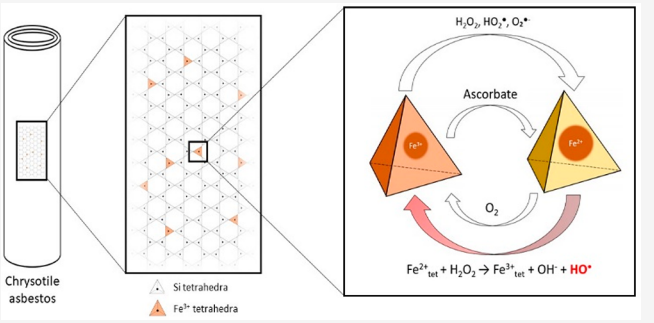

KEYWORDS: *Fiber dissolution, tetrahedral iron, carcinogenicity, hydrogen peroxide, hydroxyl radical*

INTRODUCTION

The term asbestos refers to a group of minerals that share a fibrous crystal habit and includes one serpentine mineral (chrysotile) and several amphibole minerals.[1] Asbestos has been used abundantly in industrial and consumer applications[2,3] because of its favorable physicochemical properties.[3,4] However, the use of asbestos has been banned in EU countries from the late 1980s onward[5] since, upon inhalation, the minerals can induce asbestosis, pleural diseases, lung carcinomas, and mesotheliomas.[2,6−8] The WHO-IARC classifies all asbestos minerals as carcinogenic to humans.[9] In 2014, the WHO-IPCS estimated that more than 100 000 people died of asbestos-related illnesses each year, mostly after occupational exposure.[10] Despite its severe adverse health effects, the use of asbestos has not yet been prohibited in northern American countries such as the United States and Mexico,[5] and it has even increased in some Asian countries.[11,12]

The historical use of asbestos is dominated by chrysotile (>95%), and currently only chrysotile remains in use.[13,14] Chrysotile asbestos ($Mg_3Si_2O_5(OH)_4$) consists of octahedral Mg and tetrahedral Si sheets bundling together to a fiber with an external Mg hydroxide surface.[15,16] At pH 7.4, the positively charged outermost Mg sheet dissolves within hours to days, exposing the underlying negatively charged Si sheet.[15,17] The slow dissolution kinetics of this Si sheet controls the dissolution of deeper Mg sheets.[15,17,18] Fe is substituted into the fibers' crystal structure during petrogenesis (typically 2−4 wt %) and is the most abundant redox-active metal in chrysotile.[19] Both ferrous and ferric Fe enter into octahedral sites in the Mg sheet ($Fe^{2+}{}_{oct}$ and $Fe^{3+}{}_{oct}$, respectively), whereas only ferric Fe substitutes Si in tetrahedral sites of the Si sheet ($Fe^{3+}{}_{tet}$).[18,20,21] As ferrous tetrahedral Fe ($Fe^{2+}{}_{tet}$) has a considerably larger ionic radius (63 pm) compared to Si^{4+} (26 pm) and $Fe^{3+}{}_{tet}$ (49 pm),[22] it does not enter into the Si sheet[22,23] and is consequently not detected in bulk-Fe analyses of silicates.[18,20,21,23] Proton-promoted and ligand-enhanced dissolution of $Fe^{3+}{}_{tet}$ generates vacant tetrahedral sites, which

Special Issue: Environmental Redox Processes and Contaminant and Nutrient Dynamics

Received: July 1, 2023
Revised: November 15, 2023
Accepted: November 29, 2023
Published: December 21, 2023

labilize the Si sheet of chrysotile and increase Si dissolution and, subsequently, Mg dissolution from deeper sheets.[18]

Asbestos fibers are characterized by a high biopersistence in vivo.[8,24,25] Due to the fibrous crystal habit of chrysotile asbestos, inflammatory phagocytic cells fail to phagocytose and thus remove the fibers from burdened tissues.[26] During frustrated phagocytosis, elevated amounts of enzymatically produced reactive oxygen species (ROS) like hydrogen peroxide (H_2O_2) and superoxide ($O_2^{\bullet-}$) are released into the extracellular environment.[8] Fe on fiber surfaces may interact with both these ROS to catalyze the generation of highly reactive hydroxyl radicals ($HO^{\bullet}$), which cannot be enzymatically detoxified and have a high potency to damage DNA, proteins, and lipids.[6,27−31] Fe is catalytically active because it undergoes Haber−Weiss redox cycles, in which Fe^{3+} is reduced by $O_2^{\bullet-}$ to Fe^{2+}, and Fe^{2+} is back-oxidized by H_2O_2 in the so-called Fenton reaction, yielding Fe^{3+} and $HO^{\bullet}$.[6,32] Fe^{2+} is absent on the surface of pristine chrysotile fibers.[33] However, in the presence of H_2O_2, Fe^{3+} on fiber surfaces may still engage in Haber−Weiss cycles through the Fenton-like reaction in which Fe^{3+} reacts with H_2O_2 to Fe^{2+} and hydroperoxyl ($HO_2^{\bullet}$).[34] Apart from this direct reduction of Fe^{3+} to Fe^{2+} by H_2O_2, also $HO_2^{\bullet}$ can reduce Fe^{3+} to Fe^{2+} or decompose into $O_2^{\bullet-}$, an even stronger reductant.[35] Furthermore, physiological reductants such as ascorbate[36] may reduce Fe^{3+} to Fe^{2+} and hence enable the Fenton reaction. Of note, the concentration of ascorbate in bronchoalveolar lavages is known to increase during pulmonary oxidative stress.[37]

On dissolving chrysotile surfaces at circumneutral pH, Fe^{3+}_{tet} was demonstrated to be the most efficient Fe species (on a molar basis) at catalyzing the decomposition of H_2O_2 and the only Fe species capable of catalyzing the generation of $HO^{\bullet}$ from H_2O_2.[18,38,39] During fiber dissolution at circumneutral pH, exposed Fe^{3+}_{tet} remains Fenton-active for weeks as it is embedded in the fibers' slowly dissolving Si sheets.[18] Additionally, external Fe added to chrysotile exclusively catalyzed fiber-mediated Haber−Weiss cycling when it became incorporated into vacancies in exposed Si sheets.[38] Apart from chrysotile, the exceptional redox reactivity of tetrahedral Fe (Fe_{tet}) has also been described for nontronites, in which Fe^{3+}_{tet} is preferentially reduced over octahedral Fe (Fe_{oct}), suggesting a lower redox potential of Fe_{tet} than of Fe_{oct}.[40−44]

In order to catalyze the generation of $HO^{\bullet}$, surface Fe^{3+}_{tet} first needs to be reduced to Fe^{2+}_{tet} to enable the reduction of H_2O_2 to $HO^{\bullet}$. However, so far, the presence of the Fenton-active Fe^{2+}_{tet} on chrysotile surfaces has only been postulated[38] but never experimentally established. Additionally, it remains unexplored whether redox cycling of Fe_{tet} on chrysotile surfaces accelerates Fe dissolution kinetics and subsequently promotes the labilization and dissolution of the exposed Si sheets, as observed when Fe^{3+}_{tet} undergoes proton-promoted or ligand-enhanced dissolution.[18] Increased dissolution kinetics of Fe_{tet} from chrysotile, e.g. facilitated by chelating ligands, renders fiber surfaces depleted of Fe_{tet} sites and consequently diminishes the fibers' Fenton reactivity.[18,38,39] However, it is not known whether surface depletion permanently rids the surface of Fe_{tet} or whether Fenton reactivity is recovered to some extent as fiber dissolution proceeds.

In this study, we addressed the aforementioned knowledge gaps. We hypothesized that (a) surface Fe^{3+}_{tet} can be reduced to Fe^{2+}_{tet} as a prerequisite step for the Fenton reactivity of Fe_{tet} in chrysotile.[18,38,39] Additionally, we hypothesized that (b) Fe_{tet} in exposed Si sheets of chrysotile can undergo multiple redox cycles without promoting Si dissolution. In the presence of the strong oxidant H_2O_2 we expect the residence time of Fe^{2+}_{tet} to be short, preventing reductive Fe_{tet} dissolution, the labilization of the Si surface sheet, and the consequent enhanced Si dissolution. Finally, we hypothesized that (c) chrysotile surfaces that are depleted of reactive Fe_{tet} sites (e.g., due to Fe^{3+}_{tet} removal with chelating ligands) can partly recover Fenton reactivity as fiber dissolution proceeds. This hypothesis stems from the layered structure of chrysotile fibers and the notion that upon dissolution of an Fe^{3+}_{tet}-depleted Si sheet, the underlying and newly exposed Si sheet will again contain reactive Fe^{3+}_{tet} surface sites.

These hypotheses were tested in batch dissolution experiments at the physiological lung pH of 7.4 (unless mentioned otherwise); the composition of the solution phase was analyzed by ICP-OES, and $HO^{\bullet}$ generation by chrysotile fibers was assessed by EPR spin trapping.

EXPERIMENTAL SECTION

Material. Chrysotile was purchased from Shijiazhuang Mining IMP&EXP Trade Co from China. An extensive material characterization of this chrysotile specimen has previously been reported.[18,45] Selected bulk characteristics of the Shijiazhuang chrysotile are summarized in Table 1. All chemical reagents were of p.a. quality or higher and were purchased from VWR (unless mentioned otherwise).

Table 1. Bulk Characteristics of Pristine Shijiazhuang Chrysotile Fibers[a]

	Bulk Composition	
	fusion digestion (n = 32)	NAA[b] (n = 2)
Mg (g kg^{-1})	253 (8.9)	
Si (g kg^{-1})	193 (6.4)	
Fe (g kg^{-1})	19.0 (1.2)	21.4 (0.3)
	Bulk Fe Speciation	
		Mössbauer
Fe^{2+}_{oct} (%)		38.4
Fe^{3+}_{oct} (%)		54.6
Fe^{3+}_{tet} (%)		7.0
total Fe in chrysotile (%)[c]		68.2

[a]As previously reported by Walter et al.[45] Values in parentheses represent the standard deviations. [b]Neutron activation analysis. [c]Remaining Fe is in magnetite impurities.

Experimental Strategy. The potential for redox cycling of Fe_{tet} sites on chrysotile surfaces was investigated by successively subjecting fibers to reducing and oxidizing conditions and analyzing the redox state of the surface Fe_{tet} sites by applying an Fe^{2+}-specific ligand to exclusively dissolve Fe^{2+} (including Fe^{2+}_{tet}).[33] Also, the effect of continuous Fe_{tet} redox cycling on the kinetics of proton-promoted and ligand-enhanced chrysotile dissolution was investigated by comparing dissolution in treatments with and without H_2O_2, which can both reduce and oxidize Fe_{tet} in Haber−Weiss cycles. Finally, the recovery of Fenton reactivity was examined for chrysotile from which surface-exposed Fe_{tet} had been removed through chelating ligands, by applying treatments to dissolve the exposed Fe_{tet}-depleted Si sheet.

Fiber Preconditioning. To obtain fibers with a specific surface chemistry, chrysotile was preconditioned in four different ways in accordance with Walter et al.[38,39] During preconditioning, the outermost Mg hydroxide sheet of

https://doi.org/10.1021/acsearthspacechem.3c00189
ACS Earth Space Chem. 2024, 8, 1−13

Table 2. Overview of the Various Fiber Types Used in This Study, the Corresponding Preconditioning Procedures, and a Characterization of the Fiber Surface Chemistry[a]

Chrysotile fiber type	Preconditioning procedure	Surface chemistry of fibers
pristine fibers	not applicable	unaltered—intact exposed Mg sheet
blank-altered fibers	pristine fibers incubated for 336 h in oxic blank suspensions	exposed Si sheet with Fe precipitates from the dissolved outermost Mg sheet; unaltered exposed Fe_{tet} content
DFOB-altered fibers	pristine fibers incubated for 336 h in oxic 1 mmol L^{-1} DFOB suspensions	exposed Si sheet with depleted Fe content (including $Fe^{3+}{}_{tet}$)
ascorbate-altered fibers	pristine fibers incubated for 336 h in anoxic 1 mmol L^{-1} ascorbate suspensions	exposed Si sheet with reduced Fe surface content
reoxidized ascorbate-altered fibers	ascorbate-altered fibers incubated for 24 h under air bubbling	exposed Si sheet with reoxidized Fe surface content

[a]All preconditioning procedures were conducted at pH 7.4 at a fiber to solution ratio of 1 g L^{-1}.

Table 3. Overview of the Conducted Experiments[a]

Fiber types	Treatment applied to each fiber type (per experiment)	Oxygen regime	Figure
Anoxic Dissolution Experiment			
pristine fibers	blank	anoxic	1, 2, S1
blank-altered fibers	1 mmol L^{-1} Ferr		
DFOB-altered fibers	1 mmol L^{-1} Asc		
	1 mmol L^{-1} Asc + Ferr		
Reoxidation and Rereduction Experiment			
reoxidized ascorbate altered fibers	blank	anoxic	4
	1 mmol L^{-1} Ferr		
	1 mmol L^{-1} Asc		
	1 mmol L^{-1} Asc + Ferr		
H_2O_2 Incubation Experiment			
pristine fibers	blank	oxic	5
blank-altered fibers	3.34 g L^{-1} H_2O_2		
DFOB-altered fibers	1 mmol L^{-1} DFOB		
	1 mmol L^{-1} Ferr, 3.34 g L^{-1} H_2O_2		
	1 mmol L^{-1} DFOB, 3.34 g L^{-1} H_2O_2		
$Fe^{3+}{}_{tet}$ Recovery Experiment			
DFOB-altered fibers	blank	oxic	6
	blank (pH 3.0)		

[a]All experiments were carried out at a fiber:solution ratio of 1 g L^{-1} and at pH 7.4 (unless mentioned otherwise). The denoted H_2O_2 concentrations are the starting concentrations. Ferr refers to Ferrozine, and Asc refers to ascorbate.

chrysotile dissolved, rendering fibers with an exposed Si sheet. The preconditioned chrysotile specimens mainly differed in their Fe and Si surface chemistry. Fibers depleted of surface Fe (including $Fe^{3+}{}_{tet}$) were prepared by preconditioning pristine chrysotile with 1 mmol L^{-1} desferrioxamine B (DFOB) under oxic conditions (DFOB-altered fibers). DFOB has previously been shown to effectively dissolve $Fe^{3+}{}_{tet}$ from Shijiazhuang chrysotile[18,38,39] and to generate vacant sites in the exposed Si sheet which promote Si dissolution.[18] Fibers for which the $Fe^{3+}{}_{tet}$ content of the outermost Si sheet was preserved were prepared by preconditioning pristine chrysotile in blank suspensions under oxic conditions (blank-altered fibers). Blank-altered fibers also host non-Fenton-active secondary Fe phases, such as iron (hydr)oxides on their fiber surface. These phases originated from precipitation of the octahedral Fe^{3+} content of the dissolved outermost Mg sheet. Fibers for which surface Fe^{3+} was reduced to Fe^{2+} were prepared by preconditioning pristine chrysotile with 1 mmol L^{-1} ascorbate under anoxic conditions (ascorbate-altered fibers). Finally, fibers with surface Fe sites that had undergone one full redox cycle were prepared by further incubating ascorbate-altered fibers in blank suspensions under air bubbling (reoxidized ascorbate-altered fibers). The characteristics of the various chrysotile fiber types (pristine and preconditioned) used in this study, including their preconditioning procedure and characterization of their surface chemistry, are summarized in Table 2.

Experimental Procedure. All dissolution experiments and fiber preconditioning treatments were conducted at a fiber:solution ratio of 1 g L^{-1}. 50 mmol L^{-1} of the non-metal-complexing tertiary amine ("Better") buffers[46] 3-(*N*-morpholino)propanesulfonic-acid (MOPS) and 1,4-piperazine-dipropanesulfonic acid (PIPPS) were used to maintain the pH of experimental treatments at 7.4 ± 0.3 or 3.0 ± 0.3, respectively. To compare the results of this study with previously published studies on Shijiazhuang chrysotile,[18,38,39] the ionic strength of all samples was adjusted to 300 mmol L^{-1} by addition of NaCl. In addition to the "blank" treatment (only buffer and electrolyte), other treatments included 1 mmol L^{-1} of DFOB (Novartis),[18,38] the Fe^{2+}-specific ligand Ferrozine (Sigma-Aldrich), or the reductant ascorbate. Additionally, Ferrozine and ascorbate were also applied in combination. Importantly, the pH range for which Ferrozine effectively complexes Fe^{2+} ranges from pH 3.0 to 8.0 and hence includes the pH that was used in the dissolution experiments in which Ferrozine was applied (pH 7.4).[47] In treatments involving H_2O_2, a 30% H_2O_2 stock solution (Sigma, for trace analysis) was spiked to a starting concentration of 3.3 g L^{-1} (~0.3%, i.e. ~100 mmol L^{-1}). Prior to the experiment, the concentration of the H_2O_2 stock was

https://doi.org/10.1021/acsearthspacechem.3c00189
ACS Earth Space Chem. 2024, 8, 1−13

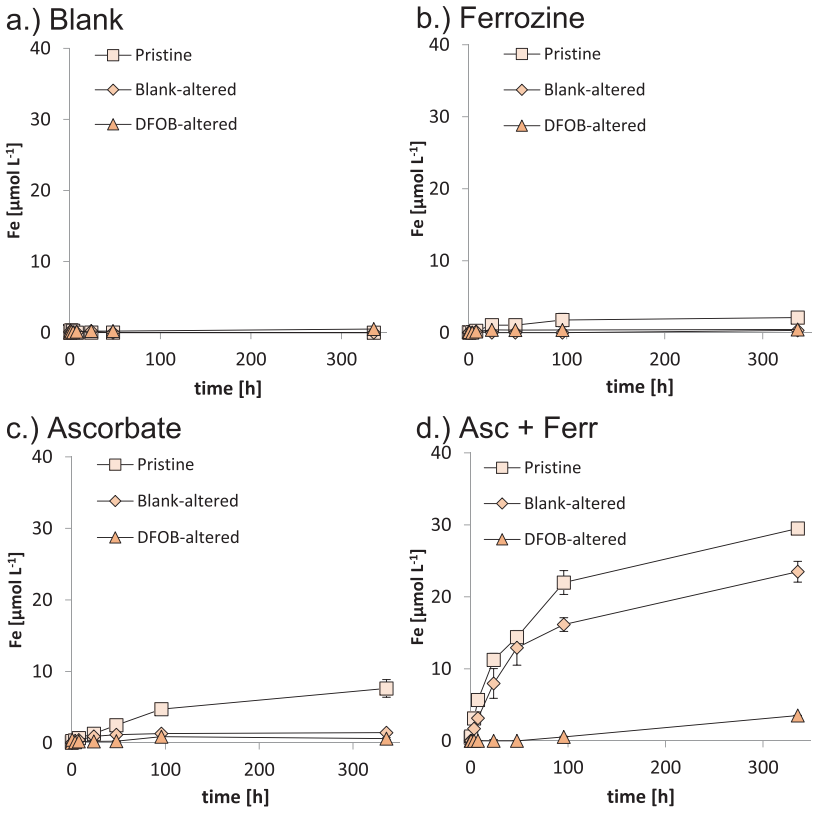

Figure 1. Mobilized Fe concentrations in anoxic incubations of pristine, blank-altered and DFOB-altered fibers at pH 7.4 in blank (a), 1 mmol L^{-1} Ferrozine (b), 1 mmol L^{-1} ascorbate (c) or 1 mmol L^{-1} ascorbate + Ferrozine (Asc + Ferr, d) suspensions. Error bars indicate standard deviations (n = 2). The Fe^{3+}_{tet} content of the chrysotile fibers in this experiment underwent half a redox cycle (reduction only) in suspensions to which ascorbate was added (c, d). The data for this figure are presented in Table S2.

determined in three $KMnO_4$ titrations to be 334 g L^{-1} (standard deviation of 2 g L^{-1}).

Preconditioning of all chrysotile types was conducted in fiber suspensions buffered at pH 7.4. The preconditioning of DFOB-altered, blank-altered, and ascorbate-altered fibers was carried out for 336 h, and the oxidation of ascorbate-altered fibers was conducted for an additional 24 h (Table 2). Table S1 lists the metal and Si concentrations mobilized during all preconditioning procedures.

In dissolution experiments and preconditioning incubations, chrysotile fibers were incubated in an end-over-end shaker at 15 rounds per minute (RPM) at 20 ± 2 °C in the dark. An exception to this was the preconditioning of reoxidized ascorbate-altered fibers, which was carried out under air bubbling and magnetic stirring at 500 rpm in a volumetric borosilicate flask. Dissolution experiments were carried out in duplicates in 15 mL PP-tubes (VWR) under anoxic or oxic conditions. Anoxic dissolution experiments were conducted in a vinyl anaerobic chamber (Coy Laboratory) filled with forming gas (with ≤3% of H_2 and O_2 contents below 1 ppm throughout the experiments). Suspensions of pristine, blank-altered, and DFOB-altered fibers were incubated at pH 7.4 in the absence (blank) or the presence of ascorbate, Ferrozine, or ascorbate + Ferrozine to examine the reduction of Fe^{3+}_{tet} surface sites on chrysotile surfaces. Additionally, also reoxidized ascorbate-altered fibers were subjected to the same treatments to examine 1 or 1.5 full redox cycles of Fe_{tet} surface sites on chrysotile fibers. Under oxic conditions, suspensions of pristine, blank-altered, and DFOB-altered fibers were incubated for 96 and 336 h at pH 7.4 in the presence of 3.3 g L^{-1} H_2O_2 (starting concentration), with or without DFOB or Ferrozine addition to examine the effect of Fe_{tet} redox cycling by H_2O_2 on proton-promoted or ligand-enhanced fiber dissolution kinetics. Additionally, oxic dissolution experiments were conducted with pristine, blank-altered, and DFOB-altered fibers at pH 7.4 without H_2O_2 addition. Finally, the anoxic ascorbate + Ferrozine and the oxic DFOB incubations of DFOB-altered fibers were also used to examine the kinetics of Fe dissolution from chrysotile fibers with exposed Si sheets depleted of Fe surface sites. Also, DFOB-altered fibers were incubated for 336 h at pH 3.0 and 7.4 in blank treatments to examine the recovery of the fibers' $HO^{\bullet}$ yield after dissolution of the exposed Fe^{3+}_{tet}-depleted Si sheet. Table 3 presents an overview of the experiments conducted for this study.

Both solution and fiber sampling were done destructively. Samples were taken after 0.5, 1, 4, 8, 24, 48, 96, 168, and 336 h. Fiber suspensions were filtered over 0.45 μm Sartorius cellulose acetate syringe filters (VWR). Aliquots of the filtrate were acidified with trace metal grade HNO_3 to 0.14 mol L^{-1}. Fibers were sampled by vacuum filtration, retained by 0.47 μm Nylon membranes (Magna) in Büchner funnels, and washed with ultrapure water to remove adsorbed free ligands or metal complexes. Subsequently, the fibers were vacuum-dried and kept in an evacuated desiccator for follow-up experiments or EPR analyses. Vacuum filtration and drying of ascorbate-altered fibers were carried out inside the anoxic glovebox to avoid oxidation of the ferrous Fe species on the chrysotile surface.

Elemental and EPR Analyses. Metal (Mg and Fe) and Si solution concentrations in preconditioning samples and samples from the dissolution experiments were determined by ICP-OES

https://doi.org/10.1021/acsearthspacechem.3c00189
ACS Earth Space Chem. 2024, 8, 1−13

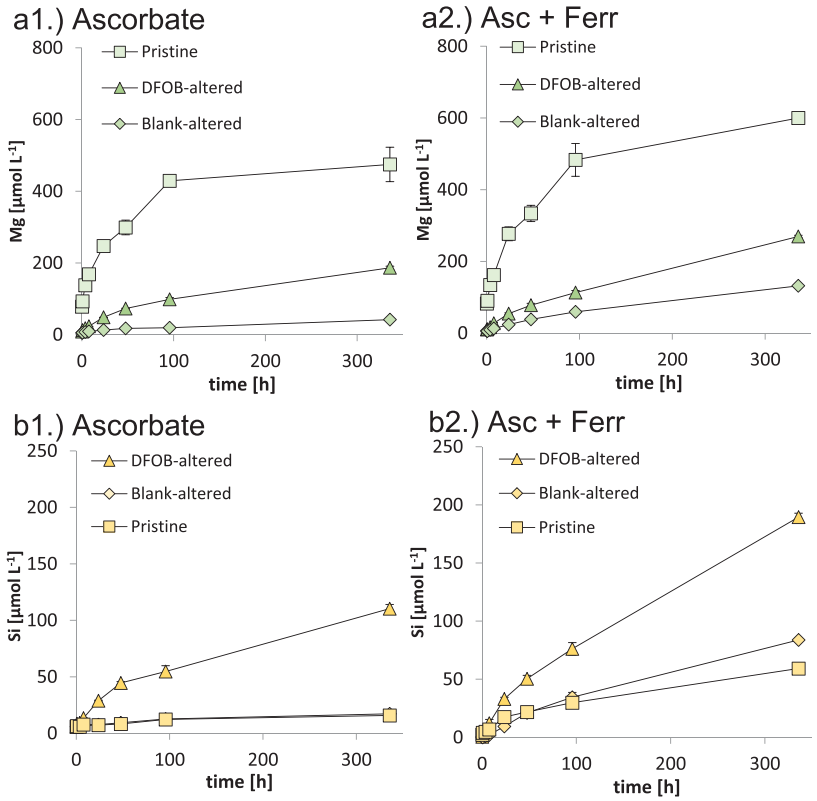

Figure 2. Mobilized Mg and Si concentrations in anoxic incubations of pristine, blank-altered, and DFOB-altered fibers at pH 7.4 in 1 mmol L^{-1} ascorbate or 1 mmol L^{-1} ascorbate + Ferrozine (Asc + Ferr) solutions. Mobilized Mg (a) and Si (b) concentrations by the ascorbate treatment are presented in subpanels 1 and 2 and by the ascorbate + Ferrozine treatment in subpanels 2. Error bars indicate standard deviations (n = 2). Results for the blank and 1 mmol L^{-1} Ferrozine treatments are presented in Figure S1. The data for this figure are presented in Table S3.

(Optima 5300-DV, PerkinElmer). Calibration standards were matrix-matched with the samples.

The generation of $HO^{\bullet}$ by pristine and incubated fiber specimens in the presence of H_2O_2 was analyzed at pH 7.4 with 5,5′-dimethyl-1-pyrroline *N*-oxide (DMPO) as the spin trap using a X-band EPR-spectrometer (Bruker EMX) and a split ring resonator (Bruker MD5). 4 replicates per treatment were analyzed. This method has been frequently applied before[18,38,39,45,48−51] and was carried out according to Walter et al.[18] The mean signal intensity (specifically the peak-to-peak intensity (I_{pp}) at the second lowest G value in the DMPO/$HO^{\bullet}$ quadruplet) of altered fibers ($\triangleq$ the decreased $HO^{\bullet}$ yield) was expressed as the percentage of the mean I_{pp} of a quadruplicate of pristine fiber replicates, which were included in each measurement session.

Data Analysis and Supplementary Data. For the statistical analysis of the EPR spin trapping results, an F-test was used to determine equal or unequal variances between samples. The analyzed samples had equal variance. Therefore, a one-way ANOVA (α = 0.05) was used to determine whether there were significant differences in EPR signal among the treatments. No subsequent posthoc tests were required.

The dissolution stoichiometry of preconditioned fibers at pH 7.4 was determined by calculating Mg and Si dissolution rates in accordance with Walter et al.[18] The surface area of the Shijiazhuang chrysotile (20.3 m^2g^{-1}) used for these calculations was reported in the same study. Only data points collected between 24 and 336 h were included for these calculations, as dissolution was closer to a steady state after the first day of the dissolution experiments. Fiber dissolution stoichiometry was evaluated by comparing the Mg_{rate}/Si_{rate} ratio with the stoichiometric bulk Mg/Si ratio of 1.5 in pristine chrysotile. For pristine fiber dissolution, no congruency calculations were performed, as dissolution of the outermost Mg sheet and Mg-containing impurities (e.g., brucite, Walter et al.[18]) introduced a bias. Finally, all analyzed data reported in Figures 1, 2, and 4−6 can be found in Tables S2−S6, respectively.

Safety Statement. No unexpected or unusually high safety hazards were encountered during the experimental work.

RESULTS

Reduction of Fe^{3+}_{tet} on Dissolving Chrysotile Surfaces. In the anoxic dissolution experiments, we studied the reduction of Fe^{3+}_{tet} to Fe^{2+}_{tet} in exposed Si sheets of chrysotile. Only submicromolar Fe concentrations were mobilized in anoxic blank suspensions of pristine, blank-altered, and DFOB-altered fibers (Figure 1a). Addition of the Fe^{2+}-specific ligand Ferrozine to these anoxic fiber suspensions did not result in a relevant increase in Fe mobilization; mobilized Fe concentrations maximally reached 2.1 μmol L^{-1} (after 336 h, for pristine fibers, Figure 1b). Addition of ascorbate to reduce the available ferric Fe surface sites on chrysotile moderately increased mobilized Fe concentrations in a pristine fiber suspension up to 8 μmol L^{-1} after 336 h of incubation (Figure 1c). However, no relevant Fe mobilization was found in anoxic suspensions of blank-altered and DFOB-altered fibers, to which ascorbate was added. Finally, Fe^{3+} reduction by ascorbate and subsequent ligand-enhanced dissolution of Fe^{2+} surface sites by Ferrozine considerably increased Fe mobilization in comparison to the previous treatments; 29.5, 23.5, and 3.5 μmol L^{-1} Fe were mobilized in

https://doi.org/10.1021/acsearthspacechem.3c00189
ACS Earth Space Chem. 2024, 8, 1−13

pristine, blank-altered and DFOB-altered anoxic chrysotile suspensions after 336 h of incubation, respectively (Figure 1d).

Mg dissolution from pristine fibers under anoxic conditions at pH 7.4 followed the two-stage dissolution model of chrysotile proposed by Walter et al.[18] In the presence of ascorbate, Mg rapidly dissolved from pristine fibers (Figure 2a1) until the outermost Mg sheet (corresponding with 406 μmol g^{-1} Mg in Shijiazhuang chrysotile[18]) had dissolved between 48 and 96 h of incubation (first stage fiber dissolution). Further Mg dissolution was hampered by the low solubility of the first exposed Si sheet (second-stage fiber dissolution). Therefore, under anoxic conditions in the presence of ascorbate, mobilized Mg concentrations from blank-altered fibers (from which the outermost Mg sheet had already dissolved during preconditioning, Table S1) remained low throughout the experiments (Figure 2a1). However, for DFOB-altered fibers, from which the outermost Mg sheet had also been dissolved, Mg dissolution was considerably higher than that for blank-altered fibers under these same conditions (Figure 2a1). This results from the labilization of the exposed Si sheet during preconditioning by DFOB-promoted Fe^{3+}_{tet} dissolution. Like for Fe mobilization (Figure 1), Ferrozine application in addition to ascorbate increased Mg dissolution from all three fiber types (Figure 2a2). Si mobilization in the presence of ascorbate was equally low from pristine and blank-altered fibers, whereas mobilized Si concentrations were clearly higher in DFOB-altered fiber treatments due to labilization of the Si sheet by DFOB preconditioning (Figure 2b1). However, when Ferrozine was additionally added to the suspensions, mobilized Si concentrations considerably increased in all three fiber treatments (Figure 2b2). For Si, this enhancing effect on dissolution of additional Ferrozine applications was more pronounced than for Mg. Mg and Si concentrations mobilized from pristine, blank-altered, and DFOB-altered fibers in anoxic pH 7.4 blank and Ferrozine-only treatments were comparable to or lower than those observed in ascorbate-only treatments (Figure S1 and Figure 2).

Congruent fiber dissolution (i.e., Mg and Si solution concentrations increasing in the stoichiometric Mg/Si ratio of chrysotile: 1.5) was observed for all anoxic incubations of preconditioned chrysotile fibers (i.e., all mineral preparations except pristine fibers) with a labilized exposed Si sheet. Specifically, dissolution was (close to) congruent for all incubations with DFOB-altered fibers (Figure 2 and Figure S1), as well as for blank-altered fibers to which ascorbate and Ferrozine were coapplied (Figure 2 and Table S7).

Finally, the addition of ascorbate to anoxic chrysotile suspensions changed the color of the fibers from brownish (as observed with pristine and blank-altered fibers) to a pale pinkish color (Figure 3 and Figure S2). DFOB-altered fibers had a whitish color, as already reported by Walter et al.[38]

Reoxidation of Fe^{2+}_{tet} and Subsequent Rereduction of Fe^{3+}_{tet} on Dissolving Chrysotile Surfaces. Figure 4 presents results from an incubation experiment in which the back-oxidation of Fe^{2+}_{tet} to Fe^{3+}_{tet} (1 redox cycle) and the subsequent rereduction of Fe^{3+}_{tet} to Fe^{2+}_{tet} (1.5 redox cycles) on chrysotile fiber surfaces were investigated. For that purpose, reoxidized ascorbate-altered fibers were incubated at pH 7.4 in either blank or Ferrozine treatment (1 redox cycle of Fe^{3+}_{tet}) and in ascorbate or ascorbate + Ferrozine treatment (1.5 redox cycles of Fe^{3+}_{tet}), respectively. The oxidation of ascorbate-altered fibers changed their color from pale pinkish to brown grayish (Figure S2b). The subsequent rereduction of reoxidized ascorbate-altered fibers by ascorbate changed the fiber color back to pale pinkish.

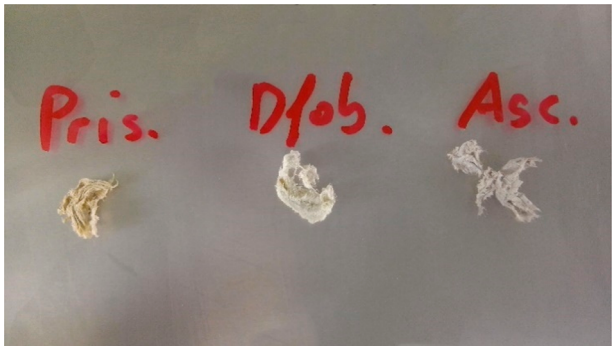

Figure 3. Observed fiber colors after different experimental incubations. From left to right: pristine fibers, DFOB-altered fibers, and ascorbate-altered fibers. The pale pinkish color of ascorbate-altered fibers was observed by incubating pristine, blank-altered, and DFOB-altered fibers at pH 7.4 in 1 mmol L^{-1} ascorbate solutions under anoxic conditions for 336 h. The color change of DFOB-altered fiber treatments from whitish to pale pinkish, however, only occurred in later stages of the incubation. Blank-altered fibers had the same color as pristine fibers (Figure S2a).

No Fe was mobilized in the blank treatment, and also, only a small amount of Fe was mobilized in the Ferrozine treatments (maximally 1.7 μmol L^{-1} after 336 h), as Fe^{2+} sites on the fiber surfaces had been back-oxidized by air bubbling during fiber preconditioning (Figure 4a). For the ascorbate treatment in which the available Fe surface sites were rereduced, a moderate increase of mobilized Fe concentrations was observed, amounting up to 3.7 μmol L^{-1} after 336 h (Figure 4a). Finally, rereduction of Fe^{3+} surface sites by ascorbate and subsequent ligand-enhanced dissolution of Fe^{2+} by Ferrozine considerably increased Fe mobilization, up to 21.8 μmol L^{-1} after 336 h (Figure 4a).

Mobilizations of Mg (Figure 4b) and Si (Figure 4c) were comparable in blank, Ferrozine, and ascorbate treatments of reoxidized ascorbate-altered fibers. In contrast, in suspensions to which ascorbate and Ferrozine were concomitantly added, considerably increased Mg and Si dissolutions were observed (Figure 4b,c, respectively). This is consistent with the increased Fe mobilization observed in this treatment (Figure 4a).

Finally, Mg dissolution in these experiments was moderately higher than that observed for blank-altered fibers incubated at pH 7.4 in anoxic (Figure S1a1) and oxic (Figure S3a) suspensions; the difference in mobilized Mg concentration after 336 h was approximately 30−40 μmol L^{-1}. This difference was also reflected in the clearly nonstoichiometric fiber dissolution for all treatments presented in Figure 4; the Mg/Si ratio was larger than 1.5, indicating an excess of Mg dissolution (Table S7).

Dissolution of Fe_{tet} from Chrysotile Surfaces by Redox Cycling. To examine whether prolonged redox cycling of Fe_{tet} in the exposed Si sheets in the presence or absence of ligands enhances chrysotile dissolution, pristine and preconditioned fibers were incubated at pH 7.4 in a ∼ 100 mmol L^{-1} H_2O_2 solution (starting concentration) with or without DFOB or Ferrozine. Under these conditions, Fe_{tet} is presumed to undergo a large number of full Haber−Weiss cycles. Mobilized Fe, Mg, and Si concentrations after 96 and 336 h were considered to establish whether the presence of H_2O_2 enhanced overall fiber

https://doi.org/10.1021/acsearthspacechem.3c00189
ACS Earth Space Chem. 2024, 8, 1−13

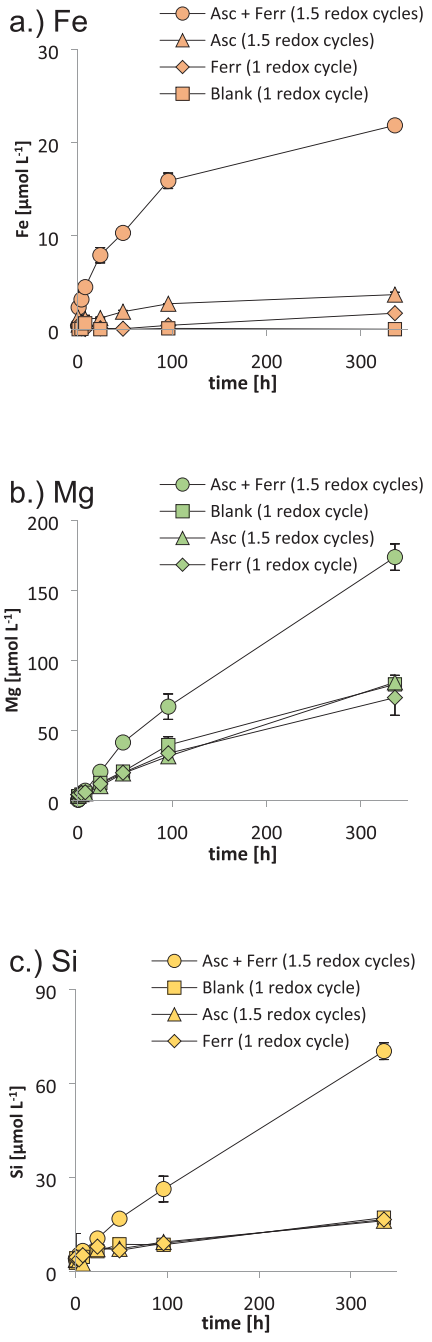

Figure 4. Fe (a), Mg (b), and Si (c) concentrations mobilized from reoxidized ascorbate-altered fibers. Fibers were incubated under anoxic conditions at pH 7.4. Blank, 1 mmol L^{-1} Ferrozine (Ferr), 1 mmol L^{-1} ascorbate (Asc), and 1 mmol L^{-1} ascorbate + Ferrozine (Asc + Ferr) treatments were applied. Error bars indicate standard deviations (n = 2). The number of redox cycles of Fe^{3+}_{tet} is noted for each treatment. The data for this figure are presented in Table S4.

dissolution by increasing proton-promoted and/or ligand-enhanced Fe_{tet} dissolution.

Mobilized Fe only exceeded low micromolar concentrations in treatments involving DFOB, and the mobilized Fe concentration was higher if in addition to DFOB also H_2O_2 was applied, except for pristine fibers after 96 h (Figure 5a1,2). Dissolved Fe concentrations in DFOB treatments increased with increasing incubation time except in pristine fiber suspensions. They were highest in suspensions of pristine fibers, which had an unaltered Fe surface content and speciation, and lowest in suspensions of DFOB-altered fibers, which were depleted in surface Fe. Fe mobilization by DFOB and H_2O_2 + DFOB in suspensions of blank-altered fibers, which contained secondary Fe phases originating from precipitation of the Fe content of the dissolved Mg sheet, was lower than in suspensions of pristine fibers. Mobilized Fe concentrations in H_2O_2 + Ferrozine treatments were as low as the concentrations in blank and H_2O_2 treatments; only in pristine fiber suspensions after 336 h was the Fe concentration mildly increased (2.7 μmol L^{-1}) (Figure 5a,b).

Mg concentrations mobilized from pristine fibers after 96 h of incubation (Figure 5b1) were largely similar in blank, H_2O_2, H_2O_2 + Ferrozine, DFOB and H_2O_2 + DFOB treatments (~400−600 μmol L^{-1}). In all treatments, the outermost Mg sheet (corresponding with 406 μmol g^{-1} Mg in Shijiazhuang chrysotile[18]) had fully dissolved. However, after 336 h, mobilized Mg concentrations were clearly elevated in the H_2O_2 + DFOB treatment (983 μmol L^{-1}) compared to all other treatments (~600 μmol L^{-1}) (Figure 5b2). Mg concentrations mobilized from blank-altered and DFOB-altered fibers successively increased from blank to H_2O_2 and H_2O_2 + Ferrozine to DFOB and ultimately to H_2O_2 + DFOB treatment; concentrations increased with the reaction time (Figure 5b1,2). Mobilized Si concentrations from pristine, blank-altered, and DFOB-altered fibers after 96 h were similar for blank, H_2O_2, and H_2O_2 + Ferrozine treatments but clearly higher in DFOB treatments and highest in H_2O_2 + DFOB treatments (Figure 5c1). After 336 h, Si dissolution of all three fiber types successively increased from blank to H_2O_2 and H_2O_2 + Ferrozine to DFOB and ultimately to H_2O_2 + DFOB treatment (Figure 5c2). Mobilized Si concentrations in the H_2O_2 + DFOB treatment exceeded 200 μmol L^{-1} in suspensions of all three fiber types.

Finally, similarly to those under anoxic conditions (Figure 2 and Figure S1), preconditioned fibers with a labilized exposed Si sheet generally dissolved congruently at pH 7.4 under oxic conditions (in the presence or absence of H_2O_2). Specifically, congruent dissolution of DFOB-altered fibers was observed in the H_2O_2, DFOB, H_2O_2 + DFOB, and H_2O_2 + Ferrozine treatments (Figure 5 and Figure S3b3 and Table S7). Also, congruent dissolution of blank-altered fibers was observed for the DFOB and H_2O_2 + DFOB treatments (Figure 5 and Figure S3b2 and Table S7). On the contrary, dissolution of blank-altered fibers in the blank, H_2O_2, and H_2O_2 + Ferrozine treatments was incongruent (Figure 5 and Figure S3a and Table S7). Interestingly, as an exception to the notion that fibers with a labilized Si sheet dissolve congruently at pH 7.4, dissolution of DFOB-altered fibers was incongruent in oxic blank treatments (Figure S3a and Table S7).

Recovery of Fenton Reactivity at Dissolving Chrysotile Surfaces. The potential recovery of the Fenton reactivity of chrysotile fibers upon dissolution of Fe^{3+}_{tet}-depleted surface Si sheets was investigated (Figure 6). Specifically, DFOB-altered fibers, which are characterized by an Fe-depleted fiber surface, were incubated at pH 7.4 and pH 3.0 in blank treatments to (partially) dissolve the exposed Fe^{3+}_{tet}-depleted Si sheet. Newly exposed Fe^{3+}_{tet} sites on the fiber surface were then indirectly identified by their Fenton reactivity in an EPR spin trapping analysis.

DFOB-altered fibers had a $HO^{\bullet}$ yield of 9% relative to pristine fibers, which is in accordance with published values for the same fiber type.[18,38,39] However, after further incubation of DFOB-

https://doi.org/10.1021/acsearthspacechem.3c00189
ACS Earth Space Chem. 2024, 8, 1−13

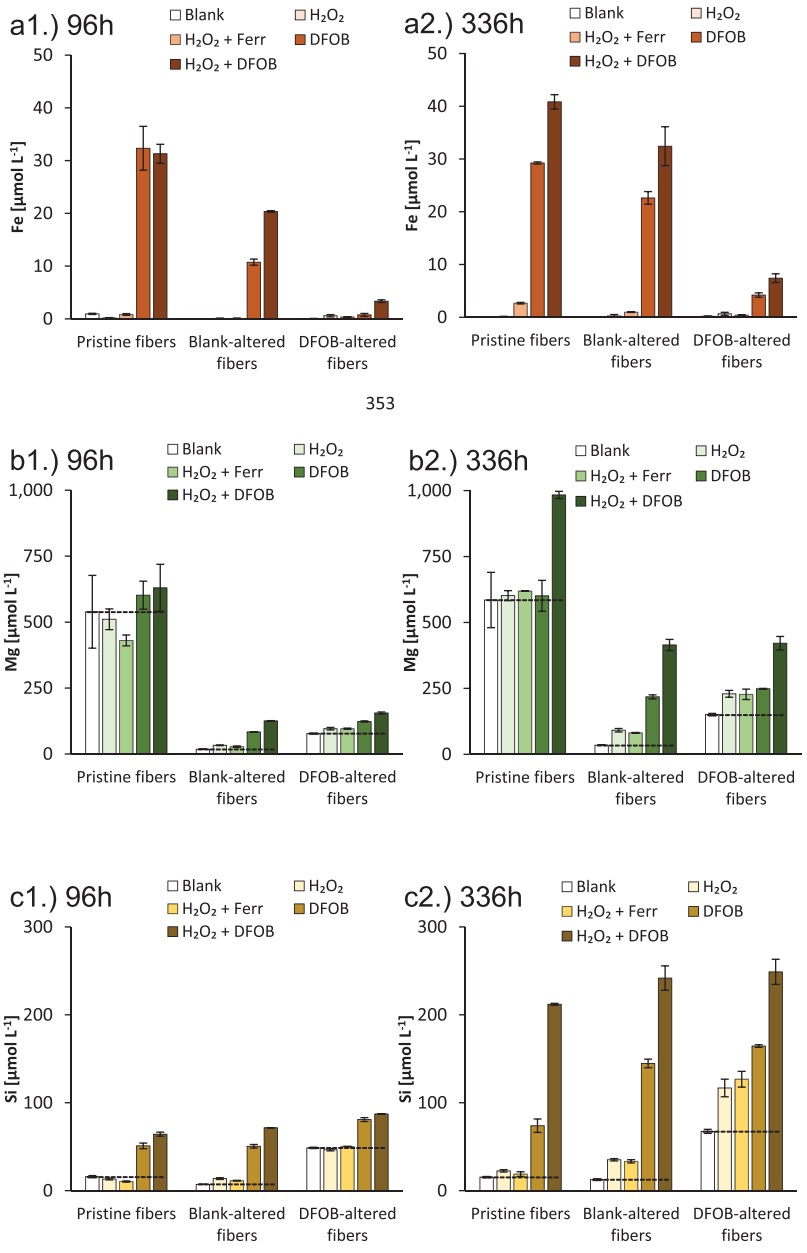

Figure 5. Fe (a), Mg (b), and Si (c) concentrations mobilized from pristine, blank-altered, and DFOB-altered fibers after 96 h (subpanels 1) and 336 h (subpanels 2) of incubation at pH 7.4 under oxic conditions in blank, 3.34 g L^{-1} H_2O_2, 3.34 g L^{-1} H_2O_2 + 1 mmol L^{-1} Ferrozine (Ferr), 1 mmol L^{-1} DFOB, and 3.34 g L^{-1} H_2O_2 + 1 mmol L^{-1} DFOB solutions. 3.34 g L^{-1} was the starting concentration of all H_2O_2 incubations. Dashed lines indicate the concentrations in the blank treatment. Error bars indicate standard deviations (n = 2). Blank and DFOB treatment data for pristine fibers were taken from Walter et al.,[18] and data for H_2O_2 treatments were taken from Walter et al.[38] The data for this figure are presented in Table S5. Mobilization of Fe, Mg, and Si by 1 mmol L^{-1} Ferrozine alone (without 3.34 g L^{-1} H_2O_2) under oxic conditions at pH 7.4 was exclusively examined for pristine fiber suspensions (1 g L^{-1}); no notable differences compared to the mobilized concentrations in the 3.34 g L^{-1} H_2O_2 + 1 mmol L^{-1} Ferrozine treatment were found (Table S8).

altered fibers for 336 h at pH 7.4, the fibers' relative $HO^{\bullet}$ yield significantly increased to 13%. However, when DFOB-altered fibers were incubated for 336 h at pH 3.0, even a 2-fold increase in relative $HO^{\bullet}$ yield, to approximately 20%, was measured.

DISCUSSION

Redox Cycling of Fe_{tet} on Dissolving Chrysotile Surfaces. Under anoxic conditions at pH 7.4, Ferrozine alone did not increase Fe mobilization above the very low micromolar or submicromolar range in suspensions of pristine and preconditioned fibers (Figure 1a,b), suggesting that the redox speciation of Fe sites on the surface of these chrysotile specimens was dominated by ferric Fe. The ascorbate treatment only led to a moderate increase of mobilized Fe^{2+} in suspensions of pristine fibers (Figure 1c). However, the concomitant addition of ascorbate and Ferrozine markedly increased Fe mobilization in suspensions of all fiber types, including DFOB-altered fibers that had been largely depleted of surface Fe during preconditioning (Figure 1d). This clearly supra-additive increase in Fe mobilization demonstrates that ascorbate reduced the Fe sites on fiber surfaces and thereby enabled ligand-enhanced Fe^{2+} dissolution by Ferrozine. The concomitant

https://doi.org/10.1021/acsearthspacechem.3c00189
ACS Earth Space Chem. 2024, 8, 1−13

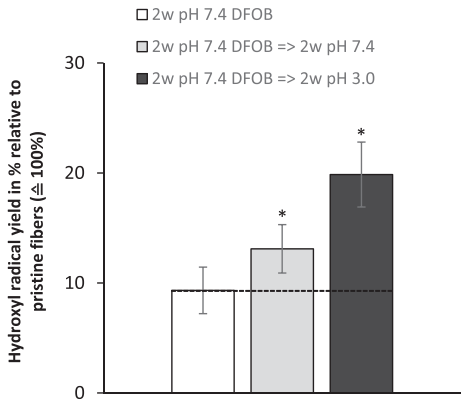

Figure 6. HO• yield in % relative to pristine fibers (≙ 100%). DFOB-altered fibers ("2w pH 7.4 DFOB") were incubated for 336 h at pH 7.4 ("2w pH 7.4 DFOB → 2w pH 7.4") and at pH 3.0 ("2w pH 7.4 DFOB → 2w pH 3.0") in blank treatments under oxic conditions. * indicates a statistically significant increase determined in an ANOVA with $p = 0.05$ relative to DFOB-altered fibers. Error bars indicate standard deviations ($n = 4$). The Mg, Si, and Fe concentrations mobilized during these incubations are presented in Table S1. The data for this figure are presented in Table S6.

addition of ascorbate and Ferrozine led to increased and stoichiometric Si and Mg dissolutions of all examined fiber types (Figure 2, Table S7). This suggests that also surface Fe^{3+}_{tet} sites were reduced to Fe^{2+}_{tet}, and that—in analogy to dissolution of Fe^{3+}_{tet} by DFOB[18]—Ferrozine dissolved Fe^{2+}_{tet} from chrysotile fiber surfaces, thereby labilizing the exposed Si sheet. This observation supports our hypothesis (hypothesis a) that Fe^{3+}_{tet} can be reduced to Fe^{2+}_{tet} on chrysotile surfaces.

The absence of enhanced fiber dissolution in anoxic ascorbate treatments implies that the surface-exposed Fe^{2+}_{tet} remained in the exposed Si sheet throughout the experiment (Figures 1c and 2a1,b1). This notion is supported by a supplementary EPR experiment in which we measured the HO• yield of blank-altered fibers that were incubated for 336 h at pH 7.4 in blank or ascorbate solutions under anoxic conditions (Figure S4). The fibers had the same HO• yield, demonstrating that reduction of Fe^{3+}_{tet} by ascorbate did not lead to the depletion of Fenton-active Fe_{tet} on the fiber surface. Also, blank-altered fibers incubated with Ferrozine under anoxic conditions had a comparable HO• yield (Figure S4), indicating that Ferrozine did not notably deplete the fiber surface from reactive Fe^{3+}_{tet} (as analogously inferred from our dissolution experiments in Figures 1 and 2 and Figure S1).

After exposing ascorbate-altered fibers with reduced Fe surface sites to oxygen (by air-bubbling) for 24 h, Ferrozine did not mobilize any Fe from the fiber specimens (reoxidized ascorbate-altered fibers). This demonstrates that after consecutive reduction and oxidation, the Fe at the chrysotile fiber surfaces again comprised ferric Fe (Figure 4a). Importantly, the Si mobilization rates for reoxidized ascorbate-altered fibers (Figure 4c) were comparable to the rates for (other) fiber types with a nonlabilized exposed Si sheet at pH 7.4, under both oxic and anoxic conditions (Table S7[18]). This indicates that one full redox cycle of the fibers' Fe^{3+}_{tet} surface sites did not lead to enhanced dissolution of Fe_{tet} with subsequent Si sheet labilization and increased Si dissolution. By incubating reoxidized ascorbate-altered fibers in anoxic ascorbate suspensions, only a moderate increase in Fe^{2+} mobilization was detected (Figure 4a). However, the combination of ascorbate + Ferrozine led to a considerable increase in Fe dissolution (Figure 4a), as the rereduction of Fe surface sites by ascorbate enabled ligand-enhanced Fe^{2+} dissolution by Ferrozine. The Fe^{2+}_{tet} dissolution from fiber surfaces thereby induced Si sheet labilization, as signified by the considerably increased Si and Mg mobilization in this treatment (Figure 4b,c and Table S7). In contrast, no Si sheet labilization was observed when reoxidized ascorbate-altered fibers were subjected to only ascorbate (Figure 4b,c, Table S7), demonstrating that also after 1.5 redox cycles Fe_{tet} was still located in the fibers' exposed Si sheet. This supports our hypothesis (hypothesis b) that Fe_{tet} can fully redox cycle in exposed Si sheets of chrysotile, without promoting Si dissolution.

It should be noted that for reoxidized ascorbate-altered fibers dissolution was not stoichiometric; the Mg/Si dissolution rate ratio was larger than 2 (Figure 4 and Table S7). Possibly, the comparatively large Mg dissolution rates were caused by accumulation of labile Mg on the fiber surfaces during the preconditioning incubations.

In the Haber–Weiss cycle, H_2O_2 both reduces and oxidizes Fe.[32] Therefore, in analogy to the observed redox cycling of Fe_{tet} induced by ascorbate and O_2, surface-exposed Fe_{tet} presumably also undergoes redox cycling in the presence of H_2O_2 at pH 7.4. This redox cycling continuously replenishes Fe^{2+}_{tet} on fiber surfaces, which, based on this and earlier studies, can be discerned as the ultimate Fenton-reactive metal species on chrysotile fiber surfaces.[18,38,39] Consequently, redox cycling of the low-abundant Fe_{tet} surface sites drives the fibers' high catalytic activity in generating HO•.[18,38,39,48−51] Apart from Fe_{tet} redox cycling by H_2O_2, also a physiological reductant such as ascorbate (as demonstrated in this study at supra-physiological concentrations), glutathione, or NADH/NADPH might reduce Fe^{3+}_{tet} sites on the surface of inhaled chrysotile fibers to Fe^{2+}_{tet} and thereby facilitate fiber-mediated Fenton reductions of H_2O_2 to HO•.

Finally, apart from structural Fe_{tet} sites on chrysotile surfaces, also other Fe species in or Fe liberated from the dissolving chrysotile surface structure may undergo redox cycling. These redox cycles presumably involve reduction of Fe^{3+}_{oct} surface sites by ascorbate and precipitation of secondary Fe minerals upon oxidation.[18,38] Since only a small amount of (pristine fibers) or no Fe (blank-altered fibers) dissolved in anoxic ascorbate treatments (Figure 1c), Fe^{2+} was largely retained, most likely by adsorbing onto the negatively charged exposed Si sheet.[15] This is supported by the approximately 20 μmol L^{-1} higher Fe concentrations in ascorbate + Ferrozine treatments after 336 h compared to the corresponding ascorbate-only treatments (Figures 1c,d and 4a).

Dissolution of Fe_{tet} from Chrysotile Surfaces through Redox Cycling. Redox cycling of Fe_{tet} up to 1.5 cycles by ascorbate and O_2 did not lead to Fe_{tet} dissolution and subsequent fiber dissolution (vide supra). However, an unknown but supposedly larger number of Fe_{tet} redox cycles by H_2O_2 increased Mg and Si dissolution, specifically in suspensions of blank-altered and DFOB-altered fibers (Figure 5b2,c2, Table S7). This falsifies our hypothesis (hypothesis b) that the redox cycling of Fe_{tet} does not increase fiber dissolution. The cause for the increased fiber dissolution in the presence of high H_2O_2 concentrations could not be established from our results. Possibly, fiber dissolution was a function of the residence time of H_2O_2 in suspension. H_2O_2 decomposition kinetics were fastest in pristine fiber suspensions and slowest in DFOB-altered fiber suspensions.[38] Correspondingly, the difference in dis-

https://doi.org/10.1021/acsearthspacechem.3c00189
ACS Earth Space Chem. 2024, 8, 1−13

solution between suspensions with and without H_2O_2 was smallest for pristine fibers and largest for DFOB-altered fibers, particularly after 336 h (Figure 5b,c). Consequently, Fe_{tet} dissolution from fiber surfaces, Si sheet labilization, and overall fiber dissolution may have scaled with the number of H_2O_2-induced Fe_{tet} redox cycles.

Under the oxic conditions of the H_2O_2 incubation experiment (Figure 5), no Fe mobilization was observed, presumably because dissolving Fe rapidly precipitated as secondary Fe minerals, as supported in a previous study with Shijiazhuang chrysotile.[18] However, precipitation of secondary Fe phases does not appear to affect redox cycling of Fe_{tet} on chrysotile surfaces; the hydroxyl radical yield of blank-altered Shijiazhuang chrysotile (which is generated by redox cycling of Fe_{tet}) did not change upon precipitation of approximately 10-fold the amount of Fe hosted in the outermost Mg and Si sheet.[38]

Interestingly, concomitant addition of H_2O_2 and DFOB to fiber suspensions led to supra-additive mobilized Fe concentrations after 336 h for all three investigated fiber types as compared to suspensions to which only H_2O_2 or DFOB was added (Figure 5a2). This suggests that redox cycling by H_2O_2 facilitated the ligand-enhanced dissolution of Fe_{tet}. This is in accordance with recent studies which demonstrate that coapplication of a reductant (ascorbate or Fe^{2+}) and DFOB to mineral suspensions facilitates ligand-controlled Fe(hydr)oxide dissolution.[52−54] The faster ligand-enhanced dissolution of Fe_{tet} by DFOB and H_2O_2 also translated into increased (and for preconditioned fibers stoichiometric) fiber dissolution rates due to increased Si sheet labilization (Figure 5b2,c2, Table S7). In contrast, redox cycling of Fe_{tet} by H_2O_2 under oxic conditions in the presence of Ferrozine did not increase the level of ligand-enhanced Fe_{tet} dissolution (Figure 5a2). Hence, it is proposed that $Fe^{2+}{}_{tet}$ on chrysotile surfaces was too short-lived to enhance ligand-enhanced dissolution during H_2O_2-induced redox cycling. Our findings suggest that the reduction of $Fe^{3+}{}_{tet}$ surface sites is the rate-limiting step in Haber−Weiss redox cycling in systems containing H_2O_2 and chrysotile fibers. This is in line with the much slower kinetics of the Fenton-like reaction (reduction of Fe^{3+}) compared to the Fenton reaction (oxidation of Fe^{2+}) as reported for other systems containing Fe and H_2O_2.[34,55,56]

Fiber dissolution by Fe_{tet} redox cycling in the presence of H_2O_2 proved slower than fiber dissolution induced by ligand-enhanced Fe_{tet} dissolution (Figures 1, 2, and 5) or by proton-promoted Fe_{tet} dissolution at more acidic pH.[18] Furthermore, a rather high H_2O_2 concentration was applied in our experiments (3.3 g L^{-1} as the starting concentration), because (patho)-physiological H_2O_2 concentrations in inflamed tissues are at least 2 orders of magnitude lower than at the beginning of our experiments.[57] Therefore, the dissolution of Fe_{tet} by H_2O_2-stimulated redox cycling is likely much slower in vivo than is observed in our experiments.

Recovery of Fenton Reactivity at Dissolving Chrysotile Surfaces. When suspending DFOB-altered fibers at pH 7.4 in a DFOB solution under oxic conditions (Figure S3b1) or in an ascorbate + Ferrozine solution under anoxic conditions (Figure 1d), initially no Fe was mobilized because the fiber surfaces had been depleted of Fe during preconditioning (Table S1). However, eventually mobilized Fe concentrations gradually increased up to approximately 4 μmol L^{-1} after 336 h. Because of the substantial mobilized Si and Mg concentrations in DFOB-altered fiber treatments (Figure 2 and Figure S3), we propose that Fe from deeper Mg and Si sheets became surface-exposed as dissolution proceeded and was consequently mobilized by the ligands. This newly surface-exposed Fe included redox-active $Fe^{3+}{}_{tet}$ from deeper Si sheets, as can be inferred from our EPR spin trapping analyses (Figure 6): by dissolving $Fe^{3+}{}_{tet}$-depleted surface sheets from DFOB-altered fibers at pH 7.4 or 3.0, the $HO^{\bullet}$ yield of the fibers increased 1.4-fold or even 2.1-fold, respectively. This demonstrates that redox-active $Fe^{3+}{}_{tet}$ sites were newly exposed at the fiber surfaces. The larger increase in relative $HO^{\bullet}$ yield of DFOB-altered fibers that had been incubated at pH 3.0 before the EPR measurements is possibly related to higher fiber dissolution rates under acidic conditions (Table S1[18]), causing a more rapid surface exposure of Fenton-active $Fe^{3+}{}_{tet}$ from deeper Si sheets. Additionally, dissolution of Fe from deeper Mg sheets and subsequent incorporation into vacancy sites in exposed Si sheets may also partly account for the observed increase in radical yield in the experiments presented in Figure 6. This is supported by a reported increase in hydroxyl radical yield upon addition of external Fe to DFOB-altered fibers.[38]

The aforementioned findings support our hypothesis (hypothesis c) that depletion of redox-active Fe_{tet} from chrysotile surfaces might only be a transient condition. This indicates that the potential of chrysotile fibers with low or depleted $Fe^{3+}{}_{tet}$ surface contents (e.g., due to fiber weathering processes) to generate $HO^{\bullet}$ can increase again as new $Fe^{3+}{}_{tet}$ surface sites become exposed while fiber dissolution proceeds. Therefore, $Fe^{3+}{}_{tet}$-depleted chrysotile fibers also remain a source of risk.

CONCLUSIONS

In this study, we demonstrate that Fe_{tet} on chrysotile surfaces can redox cycle. The ability of Fe_{tet} to fully redox cycle drives its high potency in catalyzing Haber−Weiss cycles.[18,38,39] Furthermore, our results demonstrate that redox cycling of Fe_{tet} enhances dissolution of the fibers' exposed Si sheets, but to a much smaller extent than ligand-enhanced or proton-promoted Fe_{tet} dissolution. Therefore, Fe_{tet} may redox cycle for an extended period of time in the presence of H_2O_2 in asbestos-burdened tissues, which allows fiber surfaces to continuously catalyze the generation of highly toxic $HO^{\bullet}$ from H_2O_2. For chrysotile fibers depleted in Fe_{tet} surface sites (e.g., due to selective Fe removal), our results demonstrate that new reactive surface $Fe^{3+}{}_{tet}$ sites can become freshly exposed as fiber dissolution proceeds. This implies that the reduced Fenton reactivity related to a low Fe_{tet} surface content is transient and that chrysotile remains a source of $HO^{\bullet}$ production as long as the fibers are present in vivo.

Apart from chrysotile, $Fe^{3+}{}_{tet}$ has also been detected in other pathogenic minerals such as quartz, amphiboles, and zeolites.[58−63] Hence, the redox cycling of Fe_{tet} on the mineral surface in the presence of H_2O_2 and the subsequent generation of $HO^{\bullet}$ may be a common intrinsic hazard of these pathogenic minerals. In addition to other properties such as crystal habit, the ability to generate radicals plays a key role in the toxicological potency of pathogenic minerals. In order for mineral particles to be Fenton active, tetrahedral coordination of Fe in a crystalline Si lattice may be a requirement, as illustrated by the different toxicity potentials of silica polymorphs: crystalline silica is toxic and carcinogenic to humans (WHO-IARC group 1), while amorphous silica is clearly less potent (WHO-IARC group 3).[9,64] Additionally, the crystalline and high-pressure silica-polymorph stishovite, in which Si is octahedrally coordinated, is not capable of producing radicals and seems to be non-

https://doi.org/10.1021/acsearthspacechem.3c00189
ACS Earth Space Chem. 2024, 8, 1−13

pathogenic in vitro and in vivo.[65−67] In amorphous silica and stishovite, Fe^{3+}_{tet} can crystallographically be excluded, which may, apart from other particle properties, contribute to the lesser pathogenicity of these minerals.

In conclusion, this study together with previous studies[18,38,39] supports the notion that Fe_{tet} in the exposed Si lattice of pathogenic silicate minerals such as chrysotile asbestos is the principal Fe species catalyzing particle-mediated $HO^{\bullet}$ generation at the physiological pH of 7.4, through cycling between its ferric and ferrous redox states.

■ ASSOCIATED CONTENT

Data Availability Statement

The data underlying this study are openly available in Mendeley Data at 10.17632/z4hsnd78d7.1.

Supporting Information

The Supporting Information is available free of charge at https://pubs.acs.org/doi/10.1021/acsearthspacechem.3c00189.

Fe, Mg, and Si concentrations mobilized from pristine and preconditioned fibers at pH 7.4 in anoxic blank and 1 mmol L^{-1} Ferrozine treatments, pictures of pristine and preconditioned fibers, mobilized Mg and Si concentrations in oxic blank treatments of preconditioned fibers and with mobilized Fe, Mg, and Si concentrations from pristine and preconditioned fibers in oxic 1 mmol L^{-1} DFOB treatments at pH 7.4, $HO^{\bullet}$ yields of blank-altered fibers that were incubated at pH 7.4 in anoxic blank or 1 mmol L^{-1} ascorbate or Ferrozine suspensions, Fe, Mg, and Si concentrations mobilized during fiber preconditioning, all calculated fiber dissolution rates, mobilized Fe, Mg, and Si concentrations in pristine fiber suspensions in oxic 1 mmol L^{-1} Ferrozine suspensions at pH 7.4 and data for all figures of this article and the Supporting Information (PDF)

■ AUTHOR INFORMATION

Corresponding Author

Walter D. C. Schenkeveld − *Department of Environmental Geosciences, Centre for Microbiology and Environmental Systems Science, University of Vienna, 1090 Vienna, Austria;* Present Address: Soil Chemistry and Chemical Soil Quality Group, Department of Environmental Sciences, Wageningen University, Droevendaalsesteeg 3A (Lumen building), 6708 PB Wageningen, The Netherlands; orcid.org/0000-0002-1531-0939; Email: walter.schenkeveld@wur.nl

Authors

Martin Walter − *Department of Environmental Geosciences, Centre for Microbiology and Environmental Systems Science, University of Vienna, 1090 Vienna, Austria*

Gerald Geroldinger − *Institute of Pharmacology and Toxicology, University of Veterinary Medicine, 1210 Vienna, Austria*

Lars Gille − *Institute of Pharmacology and Toxicology, University of Veterinary Medicine, 1210 Vienna, Austria*

Stephan M. Kraemer − *Department of Environmental Geosciences, Centre for Microbiology and Environmental Systems Science, University of Vienna, 1090 Vienna, Austria*

Complete contact information is available at: https://pubs.acs.org/10.1021/acsearthspacechem.3c00189

Notes

The authors declare no competing financial interest.

■ ACKNOWLEDGMENTS

The authors thank Wolfgang Obermaier and Herwig Lenitz for technical support. This research was funded by a uni:docs scholarship of the University of Vienna.

■ REFERENCES

(1) Skinner, H. C. W. Mineralogy of asbestos minerals. *Indoor. Built. Environ.* **2003**, *12*, 385−389.

(2) Liu, B.; van Gerwen, M.; Bonassi, S.; Taioli, E. Epidemiology of Environmental Exposure and Malignant Mesothelioma. *J. Thorac. Oncol.* **2017**, *12*, 1031−1045.

(3) Frank, A. L.; Joshi, T. K. The Global Spread of Asbestos. *Annals of Global Health* **2018**, *80*, 257−262.

(4) Frank, A. *History of the Extraction and Uses of Asbestos* **2005**, 1−7.

(5) Nishikawa, K.; Takahashi, K.; Karjalainen, A.; Wen, C. P.; Furuya, S.; Hoshuyama, T.; Todoroki, M.; Kiyomoto, Y.; Wilson, D.; Higashi, T.; Ohtaki, M.; Pan, G. W.; Wagner, G. Recent Mortality from Pleural Mesothelioma, Historical Patterns of Asbestos Use, and Adoption of Bans: A Global Assessment. *Environ. Health Perspect.* **2008**, *116*, 1675−1680.

(6) Hardy, J. A.; Aust, A. E. Iron in asbestos chemistry and carcinogenicity. *Chem. Rev.* **1995**, *95*, 97−118.

(7) Baur, X. Asbestos: Socio-legal and Scientific Controversies and Unsound Science in the Context of the Worldwide Asbestos Tragedy - Lessons to be Learned. *Pneumologie* **2016**, *70*, 405−412.

(8) Kamp, D. W.; Weitzman, S. A. The molecular basis of asbestos induced lung injury. *Thorax* **1999**, *54*, 638−652.

(9) WHO-IARC. Arsenic, metals, fibres and dusts. *IARC monographs on the evaluation of carcinogenic risks to humans 100 C* **2012**, 219−294.

(10) WHO-IPCS. (2014) WHO, *International programme on chemical safety: Chrysotile asbestos*.

(11) Le, G. V.; Takahashi, K.; Park, E. K.; Delgermaa, V.; Oak, C.; Qureshi, A. M.; Aljunid, S. M. Asbestos use and asbestos-related diseases in Asia: Past, present and future. *Respirology* **2011**, *16*, 767−775.

(12) Nicholson, W. J. The carcinogenicity of chrysotile asbestos - A review. *Ind. Health* **2001**, *39*, 57−64.

(13) Landrigan, P. J. Asbestos - Still a carcinogen. *N. Engl. J. Med.* **1998**, *338*, 1618−1619.

(14) *Pathology of asbestos associated diseases*; Oury, T. D., Sporn, T. A., Roggli, V. L., Eds.; Springer Berlin Heidelberg: 2014. DOI: 10.1007/978-3-642-41193-9.

(15) Bales, R. C.; Morgan, J. J. Surface-charge and adsorption properties of chrysotile asbestos in natural-waters. *Environ. Sci. Technol.* **1985**, *19*, 1213−1219.

(16) Evans, B. W. The serpentinite multisystem revisited: Chrysotile is metastable. *Int. Geol. Rev.* **2004**, *46*, 479−506.

(17) Bales, R. C.; Morgan, J. J. Dissolution kinetics of chrysotile at pH = 7 to 10. *Geochim. Cosmochim. Acta* **1985**, *49*, 2281−2288.

(18) Walter, M.; Schenkeveld, W.; Reissner, M.; Gille, L.; Kraemer, S. M. The effect of pH and biogenic ligands on the weathering of chrysotile asbestos; the pivotal role of tetrahedral Fe in dissolution kinetics and radical formation. *Chem. Eur. J.* **2019**, *25*, 3286−3300.

(19) Bowes, D. R.; Farrow, C. M. Major and trace element compositions of the UICC standard asbestos samples. *Am. J. Ind. Med.* **1997**, *32*, 592−594.

(20) Ristic, M.; Czako-Nagy, I.; Music, S.; Vertes, A. Spectroscopic characterization of chrysotile asbestos from different regions. *J. Mol. Struct.* **2011**, *993*, 120−126.

(21) Stroink, G.; Blaauw, C.; White, C. G.; Leiper, W. Mössbauer characteristics of UICC* standard reference asbestos samples. *Canadian Mineralogist* **1980**, *18*, 285−290.

(22) Shannon, R. D. Revised effective ionic radii and systematic studies of interatomic distances in halides and chalcogenides. *Acta Crystallogr., Sect. A* **1976**, *32*, 751−767.

(23) Murad, E.; Cashion, J. *Mössbauer Spectroscopy of Environmental Materials and Their Industrial Utilization*; Springer US: 2004.
(24) Mossman, B. T.; Churg, A. Mechanisms in the pathogenesis of asbestosis and silicosis. *Am. J. Respir. Crit. Care Med.* **1998**, *157*, 1666−1680.
(25) Churg, A. Deposition and clearance of chrysotile asbestos. *Ann. Occup. Hyg.* **1994**, *38*, 625−633.
(26) Aust, A. E.; Cook, P. M.; Dodson, R. F. Morphological and chemical mechanisms of elongated mineral particle toxicities. *J. Toxicol. Env. Heal. B* **2011**, *14*, 40−75.
(27) Kamp, D. W.; Graceffa, P.; Pryor, W. A.; Weitzman, S. A. The role of free-radicals in asbestos-induced diseases. *Free Radic. Biol. Med.* **1992**, *12*, 293−315.
(28) Gazzano, E.; Turci, F.; Foresti, E.; Putzu, M. G.; Aldieri, E.; Silvagno, F.; Lesci, I. G.; Tomatis, M.; Riganti, C.; Romano, C.; Fubini, B.; Roveri, N.; Ghigo, D. Iron-loaded synthetic chrysotile: A new model solid for studying the role of iron in asbestos toxicity. *Chem. Res. Toxicol.* **2007**, *20*, 380−387.
(29) Iguchi, H.; Kojo, S.; Ikeda, M. Nitric oxide (NO) synthase activity in the lung and NO synthesis in alveolar macrophages of rats increased on exposure to asbestos. *J. Appl. Toxicol. 16* **1996**, *16*, 309−315.
(30) Fenoglio, I.; Prandi, L.; Tomatis, M.; Fubini, B. Free radical generation in the toxicity of inhaled mineral particles: the role of iron speciation at the surface of asbestos and silica. *Redox Rep.* **2001**, *6*, 235−241.
(31) Winterbourn, C. C. Toxicity of iron and hydrogen peroxide: The Fenton reaction. *Toxicol. Lett.* **1995**, *82*−*83*, 969−974.
(32) Haber, F.; Weiss, J. Über die Katalyse des Hydroperoxydes. *Naturwissenschaften* **1932**, *20*, 948−950.
(33) Lund, L. G.; Aust, A. E. Iron mobilization from asbestos by chelators and ascorbic-acid. *Arch. Biochem. Biophys.* **1990**, *278*, 60−64.
(34) Neyens, E.; Baeyens, J. A review of classic Fenton's peroxidation as an advanced oxidation technique. *J. Hazard. Mater.* **2003**, *98*, 33−50.
(35) De Laat, J.; Gallard, H. Catalytic decomposition of hydrogen peroxide by Fe(III) in homogeneous aqueous solution: Mechanism and kinetic modeling. *Environ. Sci. Technol.* **1999**, *33*, 2726−2732.
(36) Hsieh, Y. H. P.; Hsieh, Y. P. Kinetics of Fe(III) reduction by ascorbic acid in aqueous solutions. *J. Agric. Food Chem.* **2000**, *48*, 1569−1573.
(37) Bui, M. H.; Sauty, A.; Collet, F.; Leuenberger, P. Dietary vitamin-c intake and concentrations in the body-fluids and cells of male smokers and nonsmokers. *J. Nutr.* **1992**, *122*, 312−316.
(38) Walter, M.; Schenkeveld, W. D. C.; Geroldinger, G.; Gille, L.; Reissner, M.; Kraemer, S. M. Identifying the reactive sites of hydrogen peroxide decomposition and hydroxyl radical formation on chrysotile asbestos surfaces. *Part. Fibre Toxicol.* **2020**, *17*, 3.
(39) Walter, M.; Schenkeveld, W. D. C.; Tomatis, M.; Schelch, K.; Peter-Vörösmarty, B.; Geroldinger, G.; Gille, L.; Bruzzoniti, M. C.; Turci, F.; Kraemer, S. M.; Grusch, M. The Potential Contribution of Hexavalent Chromium to the Carcinogenicity of Chrysotile Asbestos. *Chem. Res. Toxicol.* **2022**, *35*, 2335−2347.
(40) Russell, J. D. Infrared and Mössbauer Studies of Reduced Nontronites. *Clays Clay Miner.* **1979**, *27* (1), 63−71.
(41) Jaisi, D. P.; Kukkadapu, R. K.; Eberl, D. D.; Dong, H. Control of Fe(III) site occupancy on the rate and extent of microbial reduction of Fe(III) in nontronite. *Geochim. Cosmochim. Acta* **2005**, *69*, 5429−5440.
(42) Merola, R. B.; McGuire, M. M. Crystallographic site distribution and redox activity of Fe in nontronites determined by optical spectroscopy. *Clays Clay Miner.* **2009**, *57* (6), 771−778.
(43) Cipriano Crapina, L.; Dzene, L.; Brendlé, J.; Fourcade, F.; Amrane, A.; Limousy, L. Review: Clay-Modified Electrodes in Heterogeneous Electro-Fenton Process for Degradation of Organic Compounds: The Potential of Structural Fe(III) as Catalytic Sites. *Materials* **2021**, *14*, 7742.
(44) Chen, N.; Fang, G.; Liu, G.; Zhou, D.; Gao, J.; Gu, C. The effects of Fe-bearing smectite clays on OH formation and diethyl phthalate degradation with polyphenols and H2O2. *J. Hazard. Mater.* **2018**, *357*, 483−490.
(45) Walter, M.; Geroldinger, G.; Gille, L.; Kraemer, S. M.; Schenkeveld, W. D. C. Soil-pH and cement influence the weathering kinetics of chrysotile asbestos in soils and its hydroxyl radical yield. *J. Hazard. Mater.* **2022**, *431*, No. 128068.
(46) Kandegedara, A.; Rorabacher, D. B. Noncomplexing tertiary amines as "better" buffers covering the range of pH 3−11. Temperature dependence of their acid dissociation constants. *Anal. Chem.* **1999**, *71*, 3140−3144.
(47) Yang, Z.; Yan, Y.; Yu, A.; Pan, B.; Pignatello, J. J. Revisiting the phenanthroline and Ferrozine colorimetric methods for quantification of Fe(II) in Fenton reactions. *J. Chem. Eng.* **2020**, *391*, No. 123592.
(48) Fubini, B.; Mollo, L.; Giamello, E. Free-radical generation at the solid/liquid interface in iron-containing minerals. *Free Radic. Res.* **1995**, *23*, 593−614.
(49) Favero-Longo, S.; Turci, F.; Tomatis, M.; Compagnoni, R.; Piervittori, R.; Fubini, B. The Effect of Weathering on Ecopersistence, Reactivity, and Potential Toxicity of Naturally Occurring Asbestos and Asbestiform Minerals. *J. Toxicol. Environ. Health, Part A* **2009**, *72*, 305−314.
(50) Fubini, B.; Mollo, L. Role of iron in the reactivity of mineral fibers. *Toxicol. Lett.* **1995**, *82*−*83*, 951−960.
(51) Turci, F.; Favero-Longo, S. E.; Tomatis, M.; Martra, G.; Castelli, D.; Piervittori, R.; Fubini, B. A biomimetic approach to the chemical inactivation of chrysotile fibres by lichen metabolites. *Chem. - Eur. J.* **2007**, *13*, 4081−4093.
(52) Kang, K.; Schenkeveld, W. D. C.; Biswakarma, J.; Borowski, S. C.; Hug, S. J.; Hering, J. G.; Kraemer, S. M. Low Fe(II) Concentrations Catalyze the Dissolution of Various Fe(III) (hydr)oxide Minerals in the Presence of Diverse Ligands and over a Broad pH Range. *Environ. Sci. Technol.* **2019**, *53*, 98−107.
(53) Biswakarma, J.; Kang, K.; Borowski, S. C.; Schenkeveld, W. D. C.; Kraemer, S. M.; Hering, J. G.; Hug, S. J. Fe(II)-Catalyzed Ligand-Controlled Dissolution of Iron(hydr)oxides. *Environ. Sci. Technol.* **2019**, *53*, 88−97.
(54) Wang, Z.; Schenkeveld, W. D. C.; Kraemer, S. M.; Giammar, D. E. Synergistic Effect of Reductive and Ligand-Promoted Dissolution of Goethite. *Environ. Sci. Technol.* **2015**, *49*, 7236−7244.
(55) Kaźmierczak-Barańska, J.; Boguszewska, K.; Adamus-Grabicka, A.; Karwowski, B. T. Two Faces of Vitamin C-Antioxidative and Pro-Oxidative Agent. *Nutrients* **2020**, *12*, 1501.
(56) Wang, S. A Comparative study of Fenton and Fenton-like reaction kinetics in decolourisation of wastewater. *Dyes Pigm.* **2008**, *76*, 714−720.
(57) Sies, H. Hydrogen peroxide as a central redox signaling molecule in physiological oxidative stress: Oxidative eustress. *Redox Biol.* **2017**, *11*, 613−619.
(58) Roquemalherbe, R.; Diazaguila, C.; Reguerariuz, E.; Fundoralliteras, J.; Lopezcolado, L.; Hernandezvelez, M. The state of iron in natural zeolites - A Mossbauer study. *Zeolites* **1990**, *10*, 685−689.
(59) Di Benedetto, F.; D'Acapito, F.; Fornaciai, G.; Innocenti, M.; Montegrossi, G.; Pardi, L. A.; Tesi, S.; Romanelli, M. A Fe K-edge XAS study of amethyst. *Phys. Chem. Miner.* **2010**, *37*, 283−289.
(60) Weil, J. A. EPR of iron centers in silicon dioxide. *Appl. Magn. Reson.* **1994**, *6*, 1−16.
(61) Dennen, W. H. Stoichiometric substitution in natural quartz. *Geochim. Cosmochim. Acta* **1966**, *30*, 1235−1241.
(62) Goldfarb, D.; Strohmaier, K. G.; Vaughan, D. E. W.; Thomann, H.; Poluektov, O. G.; Schmidt, J. Studies of framework iron in zeolites by pulsed ENDOR at 95 GHz. *J. Am. Chem. Soc.* **1996**, *118*, 4665−4671.
(63) Luys, M.-J.; De Roy, G. L.; Adams, F.; Vansant, E. F. Cation site population in amphibole asbestos. A Mossbauer study. *J. Chem. Soc., Faraday Trans* **1983**, *79*, 1451−1459.
(64) WHO-IARC.. Silica, some silicates, coal dust and paramid fibrils. *IARC monographs on the evaluation of carcinogenic risks to humans* **1997**, *68*, 1−475.

(65) Cerrato, G.; Fubini, B.; Baricco, M.; Morterra, C. Spectroscopic, structural and microcalorimetric study of stishovite, a non-pathogenic polymorph of SiO2. *J. Mater. Chem.* **1995**, *5*, 1935−1941.
(66) McQueen, C. A. 8.17 - Crystalline Silica and Silicosis A2. In *Comprehensive Toxicology*, 2nd ed.; Driscoll, K. E., Guthrie, G. D., Eds.; Elsevier: 2010; pp 331−350.
(67) Bríeger, H.; Gross, P. On the Theory of Silicosis, II. Stishovite. *Arch. Environ. Health* **1967**, *15*, 751−757.

https://doi.org/10.1021/acsearthspacechem.3c00189
ACS Earth Space Chem. 2024, 8, 1−13